THE JOURNAL OF PHYSICAL CHEMISTRY C

Article

pubs.acs.org/JPCC

Coherent Control of Colloidal Semiconductor Nanocrystals

M. Ruge,[†] R. Wilcken,[†] M. Wollenhaupt,[†] A. Horn,[†,‡] and T. Baumert*,[†]

[†]Institute of Physics, Center for Interdisciplinary Nanostructure Science and Technology (CINSaT), University of Kassel, Heinrich-Plett-Strasse 40, D-34132 Kassel, Germany

[‡]Laser Zentrum Hannover e.V., Semiconductor and Photovoltaics-Group, Hollerithallee 8, D-30419 Hannover, Germany

ABSTRACT: Weak-field coherent control of a two-photon transition in colloidal semiconductor nanocrystals (NCs) by tailored femtosecond laser pulses is demonstrated at room temperature. Ensembles of cadmium sulfide (CdS) and cadmium selenide (CdSe) NCs forming a colloidal suspension were irradiated by ultrashort infrared laser pulses being phase-modulated in frequency domain. The luminescence generated by electron−hole recombination after two-photon excitation (TPE) of the shaped pulses serves as a measure for NC excitation. In the experiment, we applied polynomial spectral phase functions of second- (GDD) and third-order (TOD), as well as phase jumps (θ-step), and studied the effect of the various shaped laser pulses on the excitation of both types of NCs. In view of potential applications in multilabel two-photon microscopy, both types of NCs are uniformely mixed in a single sample. We find that distinct pulse shapes enable selectivity among the excitation of both NC types in this mixture. Numerical simulations based on calculating the spectral overlap of the second order nonlinear optical spectrum and the TPE spectrum of the NCs are in good agreement with the measurement results. Analytic expressions derived for the second order power spectral density (PSD) because of combined GDD-TOD modulation and the θ-step rationalize this finding and show that GDD-TOD modulation provides a spectroscopic tool to investigate the TPE spectrum.

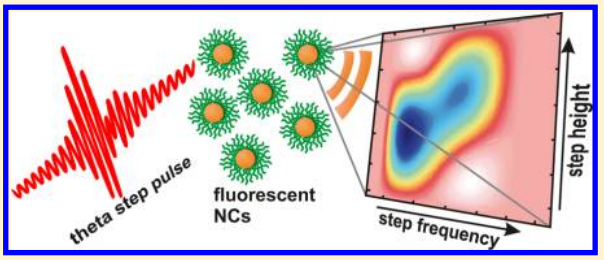

INTRODUCTION

Time domain investigations of the fundamental interplay between light and molecular dynamics first became feasible with the availability of ultrashort laser pulses.[1] Numerous concepts of coherent control (CC) operative in different intensity regimes ranging from the weak- to the intermediate- and strong-[2−4]field regime have been investigated extensively on different quantum systems. In the pertubative regime, interferences of multiple excitation pathways enable control.[5−8] This approach was demonstrated mainly on atoms in the gas phase. Some CC schemes were proven to be operative in the liquid phase[9−13] as reviewed in ref 14. In this context the properties of femtosecond laser pulses were also exploited as a spectroscopic tool for the investigation of large biomolecules[15−17] and PbS NCs.[18]

For one thing, CC of semiconductor nanocrystals (NCs) is of interest because of their atom-like level structure and for another, NCs have received considerable attention due to their applications in devices, such as diodes, lasers, and solar cells,[31] and novel microscopy techniques. Coherent control on NCs has already been reported[19] but was applied to single NCs in most cases. In order to reduce decoherence phenomena recent CC experiments on quantum dots have been performed at cryogenic temperatures. However, room temperature control scenarios would be beneficial for many technical and biological applications that are usually operated under ambient conditions. For example, NCs have emerged as a photostable biolabel in confocal microscopy, as well as in two-photon microscopy.[20,21] For the latter, contrast generation by manipulation of the spectral phase of an exciting laser pulse is a promising application for coherent control. This technique is affected usually by homogeneous and inhomogeneous broadening, both present in NC samples. As a consequence robust control scenarios, which take typical variations in transition energies because of the NCs size distribution into account are required.

In this contribution, we examine CC on colloidal CdSe and CdS NCs under ambient conditions. The CC scheme presented exploits modest differences in the two-photon excitation spectra in order to achieve selective excitation. This contribution is organized as follows: In the Properties of the System and Its Interaction with Shaped Pulses section the two-photon excitation mechanism in analogy to established techniques in atomic physics is described. In the Analytic Derivation of Second-Order Power Spectral Density (PSD) section, we derive analytic expressions to quantitatively describe the key aspects of the phase functions responsible for the achieved selectivity. In the Experimental Section, a brief description of CdS and CdSe NC synthesis, NC mixture preparation, and of our two-photon excitation experiment is given. In the Results and Discussion section, the influence of two spectral phase modulation functions on the excitation of the two types of NCs is presented and discussed in terms of the nonlinear second-order spectrum of the phase modulated

Received: January 29, 2013
Revised: May 2, 2013
Published: May 3, 2013

   dx.doi.org/10.1021/jp4010136 | J. Phys. Chem. C 2013, 117, 11780−11790

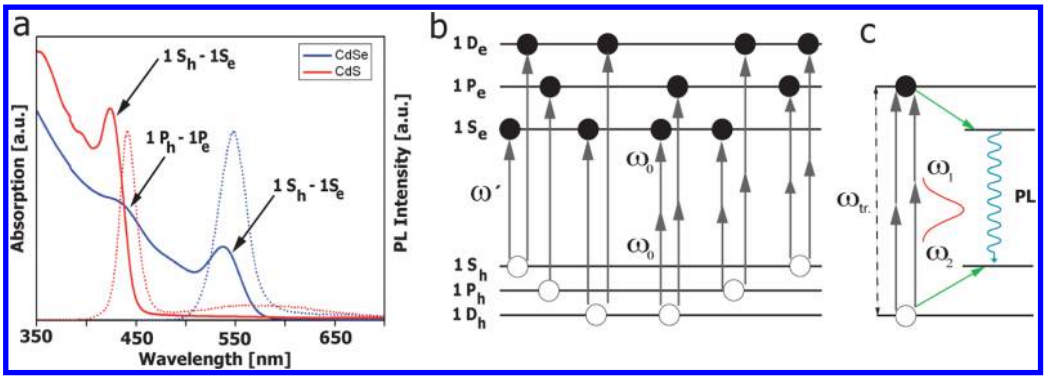

Figure 1. (a) Linear absorption (full lines) and photoluminescence (PL) spectra (dashed lines) of our synthesized CdS and CdSe NCs dispersed in *n*-hexane with diameters 4.2 and 2.9 nm. The optical interband one-photon transitions involved are indicated by arrows in the absorption spectra. (b) Simplified energy level diagram of semiconductor NCs displaying electron and hole levels.[22] One-photon ω' and two-photon $2\omega_0$ transitions in semiconductor NCs address different manifolds of states. (c) Two-photon excitation mechanism with a broadband laser pulse. An interband two-photon transition which creates an exciton in the quantum dot is induced for all photon pairs matching a transition frequency $\omega_1 + \omega_2 = \omega_{tr.}$. After excitation the electron (hole) relaxes nonradiatively to the bottom of the conduction-band $1S_e$ (to the top of the valence $1S_h$), where radiative recombination occurs.

fundamental laser spectrum and the two-photon excitation spectra of the NCs in refs 30 and 31. For comparison with the experimental findings, control landscapes based on this two-photon spectra appoximated with linear functions of different slopes are computed. To assess the selectivity in the excitation, the contrast for the excitation of the different NC types in the mixture obtained with each phase function is quantified.

PROPERTIES OF THE SYSTEM AND ITS INTERACTION WITH SHAPED LASER PULSES

Semiconductor Nanocrystals. If the dimensions of a semiconductor are reduced to a size comparable to the exciton Bohr radius of the material, the electron can no longer be regarded as quasi-free because of quantum confinement.[22] If the size reduction is performed in all three dimensions, the resulting structure is called quantum dot or nanocrystal (NC). The most important property of quantum confined species is the presence of size-dependent energy levels in the conduction and valence bands of the crystal. The exact position of these energy levels depends on the quantum dot size, the band gap of the bulk semiconductor and the band structure of the latter. Photon absorption generates an electron hole-pair and thus promotes an electron from a valence band level to a conduction band level. For interband one-photon transitions, the change in the angular momentum quantum numbers is $\Delta L = 0, \pm 2$ and two-photon transitions satisfy $\Delta L = \pm 1, \pm 3$.[23,24] Thus the energy level structure is imprinted on the optical spectra of the quantum dots. Because of the different selection rules, one- and two-photon spectroscopy provides complementary information. The CdS and CdSe NCs synthesized in the course of this study belong to the II−VI-semiconductor compounds, where the exciton Bohr radius is 2.5 nm in CdS and 4.8 nm in CdSe,[25] respectively. The diameters of our NCs are 4.2 and 2.9 nm as determined experimentally by linear absorption spectroscopy as shown in Figure 1a (further details will be given in the Synthesis of Semiconductor Nanocrystals and Sample Preparation section), thus their sizes are comparable to the exciton Bohr radius of the materials, which means that the electron is strongly confined in both types of NCs. In addition, the size determination allows us to use the (size-dependent) two-photon spectra already reported in the literature for our simulations.

Different states accessible by one and two photons are illustrated by means of a simplified energy level diagram (Figure 1b). The single arrows correspond to one-photon transitions assigned in the linear spectra at the one-photon transition frequency ω', whereas the double arrows indicate possible two-photon transitions at the two-photon transition frequency $2\omega_0$. Note that these transitions are not observed in the one-photon absorption spectra. This is in contrast to organic non-centrosymmetric dyes, where transitions can occur between many states being mediated by less restrictive selection rules.[26] Experimentally this manifests in the similarity of one- and two-photon excitation spectra of several dyes in the spectral window between 700 and 900 nm.[13] In contrast to the excitation spectrum, the photoluminescence (PL) spectrum of quantum dots originating from two-photon excitation is identical to the case of one-photon excitation. Even if an electron (a hole) was promoted to an energetically higher lying level, relaxation to the bottom of the conduction band (the top of the valence band) occurs. Thus, recombination luminescence is always observed from the energetically lowest lying level (Figure 1c).[27] Therefore the PL spectrum shown in Figure 1a is similar to the one observed in the case of two-photon excitation. All PL signals detected in our experiment, arise from transitions between electron and hole states, that is, excitonic states which have been studied extensively and recently reviewed in.[28] In general some nonlinear properties of NCs arise from biexcitons, generated by simultaneous absorption of two photons with high photon energies.[29] However, the excitation mechanism in our experiment is different, because the single photon energies of around 1.5 eV, are well below the bandgap energy of CdSe and CdS NCs involving virtual intermediate states within the bandgap. This kind of two-photon excitation was investigated in[30,31] and the results (wavelength dependent TPE cross sections) reveal the structure of two-photon addressable states, without an (real) intermediate state. These TPE cross sections are used for our simulations and verify the two-photon excitation mechanism (Figure 1c).

Pulse Shaping. The excitation of multiphoton transitions with broadband laser pulses can be controlled via higher-order spectral interference,[7,8] that is, the quantum interference of the various pathways provided by different combinations of spectral components in the pulse (Figure 1c). In the following, we

dx.doi.org/10.1021/jp4010136 | J. Phys. Chem. C 2013, 117, 11780−11790

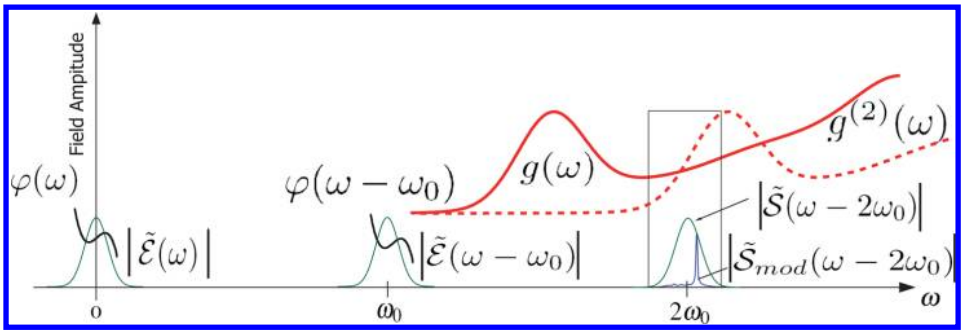

Figure 2. Frequency domain representation of CC on CdS NCs. One-photon $g(\omega)$ (red solid) and two-photon $g^{(2)}(\omega)$ (red dashed) excitation spectra are depicted for comparison. The real valued electric field $E(t)$ oscillating with the carrier frequency ω_0 is related to the spectrum $\tilde{\mathcal{E}}(\omega-\omega_0)$. The second-order spectrum $\tilde{S}_{\mathrm{mod}}(\omega-2\omega_0)$ has a nonvanishing contribution centered around $2\omega_0$. Introducing the spectral phase $\varphi(\omega-\omega_0)$ to the fundamental field $\tilde{\mathcal{E}}(\omega-\omega_0)$ yields an amplitude- and phase-modulated second-order spectrum $\tilde{S}(\omega-2\omega_0)$, which is used to control the two-photon transition. The frame highlights the region of the inhomogenous-broadened and two-photon addressable excitonic peak of the CdS NC ensemble, depicted quantitatively in Figure 3.

describe the two-photon excitation of NCs with spectrally modulated fs laser pulses.[35,36] The slowly varying temporal envelope $\mathcal{E}(t)$ of an ultrashort laser pulse is related to the spectrum $\tilde{\mathcal{E}}(\omega)$ by Fourier-transform. The fast oscillating electric field reads $E(t) = \mathcal{E}(t)e^{i\omega_0 t}$ with the corresponding spectrum $\tilde{\mathcal{E}}(\omega-\omega_0)$ where ω_0 is the laser central frequency. Introducing the spectral phase modulation function $\varphi(\omega)$, the modulated spectrum of the envelope reads $\tilde{\mathcal{E}}_{\mathrm{mod}}(\omega) = \tilde{\mathcal{E}}(\omega)e^{-i\varphi(\omega)}$. The envelope of the second order optical spectrum of the modulated pulse ($\tilde{S}_{\mathrm{mod}}(\omega)$) is obtained by self-convolution[7,37]

$$\tilde{S}_{\mathrm{mod}}(\omega) \propto \int_{-\infty}^{+\infty} \tilde{\mathcal{E}}_{\mathrm{mod}}\left(\frac{\omega}{2}+\Omega\right)\tilde{\mathcal{E}}_{\mathrm{mod}}\left(\frac{\omega}{2}-\Omega\right) \mathrm{d}\Omega \tag{1}$$

$$= \int_{-\infty}^{+\infty} \tilde{\mathcal{E}}\left(\frac{\omega}{2}+\Omega\right)\tilde{\mathcal{E}}\left(\frac{\omega}{2}-\Omega\right) e^{-i[\varphi(\frac{\omega}{2}+\Omega)+\varphi(\frac{\omega}{2}-\Omega)]}\,\mathrm{d}\Omega \tag{2}$$

The spectrum of the envelope $\tilde{S}_{\mathrm{mod}}(\omega)$ is shifted by $2\omega_0$ to yield the second order optical spectrum $\tilde{S}_{\mathrm{mod}}(\omega-2\omega_0)$, which is relevant for control of the two-photon transition (Figure 2). By spectral phase modulation of the first-order spectrum, the amplitude and phase of the second-order field are modulated. Thereby the spectral energy of the second-order field is concentrated at the desired transition.[5] The two-photon fluorescence signal $S^{(2)}$ is proportional to the overlap of the NC's two-photon excitation (TPE) spectrum $g^{(2)}(\omega)$ and the second order power spectral density (PSD), that is, $\tilde{I}_{\mathrm{mod}}(\omega-2\omega_0) = |\tilde{S}_{\mathrm{mod}}(\omega-2\omega_0)|^2$ and reads[7]

$$S^{(2)} \propto \int_{-\infty}^{+\infty} g^{(2)}(\omega)\tilde{I}_{\mathrm{mod}}(\omega-2\omega_0)\,\mathrm{d}\omega \tag{3}$$

To elucidate the CC scenario, the frequency domain representation of the above quantities is depicted in Figure 2.

As a consequence of selection rules the two-photon transitions in NCs occur at higher energies (frequencies) compared to the corresponding one-photon transitions.[23] Since the two-photon excitation spectra of CdSe and CdS NCs are different in the spectral region around $2\omega_0$ (Figure 3), selectivity in the excitation of the NCs is achieved by tailoring the second-order spectrum $\tilde{S}_{\mathrm{mod}}(\omega-2\omega_0)$. To quantify the

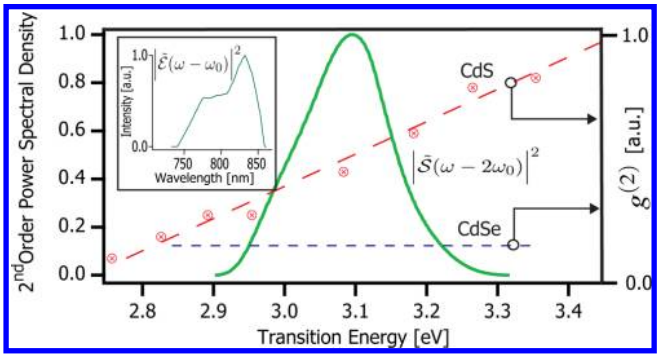

Figure 3. Illustration of eq 3, exemplified for the unmodulated (TL) pulse. The two-photon excitation spectra of CdS (red dashed line) and CdSe NCs (blue dashed line) are shown along with the calculated second-order spectrum $|\tilde{S}(\omega-2\omega_0)|^2$ (green solid line) of the transform-limited pulse. The latter was calculated from the measured fundamental laser spectrum $|\tilde{\mathcal{E}}(\omega-\omega_0)|^2$ (inset). Phase modulation of $\tilde{\mathcal{E}}(\omega-\omega_0)$ results in an amplitude modulation of $|\tilde{S}(\omega-2\omega_0)|^2$ as depicted at the top of Figures 6 and 7 and for a Gaussian fundamental spectrum in Figure 4. The resulting signal $S^{(2)}$ of the two NC types is proportional to the overlap of $\tilde{S}_{\mathrm{mod}}(\omega-2\omega_0)$ and the two-photon excitation spectra, related either to CdSe or CdS NCs.

selective excitation, we define the contrast of the respective two-photon PL signals

$$C = \frac{S^{(2)}(\omega)_{\mathrm{CdSe}} - S^{(2)}(\omega)_{\mathrm{CdS}}}{S^{(2)}(\omega)_{\mathrm{CdSe}} + S^{(2)}(\omega)_{\mathrm{CdS}}} \tag{4}$$

In the experiment, the concentrations of CdSe and CdS NCs in the mixture are chosen such as to provide PL signals of approximately the same magnitude for the bandwidth-limited (unmodulated) IR pulse (see Experimental Section). Consequently the contrast obtained for the transform limited pulse is zero. To assess the amplitude of the variation of the contrast C, we study two distinctly parametrized spectral phase modulation functions. The first one is a constant phase with a discontinuity at a certain frequency, whereas the second one is a polynomial phase modulation function.

Spectral Phase Modulation. The first modulation function is the step-modulation, which is characterized by a jump of the spectral phase at the step-frequency ω_{step}.[7,8,38]

dx.doi.org/10.1021/jp4010136 | J. Phys. Chem. C 2013, 117, 11780−11790

$$\varphi_{\text{step}}(\omega) = \frac{\theta}{2}\sigma(\omega - \omega_{\text{step}}) \tag{5}$$

The signum function $\sigma(\omega)$ is defined to be ± 1 for ω greater than or less than 0, respectively, resulting in a discrete jump of the spectral phase from $-\theta/2$ to $\theta/2$. Step modulation is a standard tool in CC[7,8] and has been recently also applied in ref 39 to scan across the TPE spectrum of an organic dye.

To efficiently scan the TPE spectra of the NCs, we introduce the second spectral modulation function that makes use of a combination of second- and third-order dispersion.[36]

$$\varphi_{\text{GDD-TOD}}(\omega) = \varphi_{\text{GDD}}(\omega) + \varphi_{\text{TOD}}(\omega) \tag{6}$$

with

$$\varphi_{\text{GDD}}(\omega) = \frac{1}{2}\phi_2(\omega - \omega_0)^2 \tag{7}$$

and

$$\varphi_{\text{TOD}}(\omega) = \frac{1}{6}\phi_3(\omega - \omega_0)^3 \tag{8}$$

A detailed discussion of its temporal pulse shape is given in ref 33. Using the phase functions defined above, the signal $S^{(2)}$ (eq 3) depends on the two phase modulation parameters in eqs 5 and 6 and is termed $S^{(2)}(\omega_{\text{step}},\theta)$ for the step-modulation and $S^{(2)}(\phi_2,\phi_3)$ for the combined GDD−TOD phase modulation, respectively. [For clarity, we distinguish between the spectral phase modulation *function* (e.g., $\varphi(\omega)$) and the modulation *parameter* of this function ϕ_2. Occasionally both the group delay dispersion function $\text{GDD}(\omega) = d^2/d\omega^2\varphi(\omega)$ and the modulation parameter ϕ_2 are referred to as GDD. However only in the special case of purely second-order spectral phase modulation when $\varphi(\omega) = 1/2\phi_2(\omega - \omega_0)^2$ and thus $\text{GDD}(\omega) = \phi_2$, both quantities are identical. Nevertheless, for brevity, we shall use the terms GDD- and TOD-modulation for combined spectral phase modulation with $\varphi_{\text{GDD}}(\omega)$ and $\varphi_{\text{TOD}}(\omega)$ as defined in eq 8 synonymously.] Analytic expressions for the relevant second-order power spectral density of the modulated pulses are described in the next section.

Simulation of the Spectral Phase-Dependent Signal. To model the interaction of shaped laser pulses with nanocrystals accurately, eq 3 is evaluated numerically. The two relevant quantities in eq 3 are the experimentally measured and intensity-calibrated fundamental laser spectrum $|\tilde{\mathcal{E}}(\omega - \omega_0)|^2$ (inset to Figure 3) and the intrinsic TPE spectrum of CdSe and CdS NCs, related to the TPE cross section, investigated in refs 30 and 31. $g^{(2)}(\omega)$ of the NCs is derived from the data points reported in ref 30. The wavelength scale [nm] was converted to units of transition energy in [eV] or in frequency [rad/fs]. To quantify the increase in two-photon excitation toward higher transition energies a linear fit (red dashed line) to this data points was performed. The slope was used to evaluate eq 3 to represent the signal from CdS NCs. In the case of CdSe NCs a rather uniform excitation (dashed blue line) was reported in ref 31, therefore no fitting procedure for slope determination was required. The two-photon excitation spectra for CdS and CdSe NCs are shown in Figure 3 along with the calculated second-order power spectral density (PSD) of the transform-limited pulse $|\tilde{\mathcal{S}}(\omega - 2\omega_0)|^2$ derived from the measured fundamental laser spectrum.

In contrast to their one-photon counterparts (Figure 1), no excitonic peaks are observed in the two-photon excitation spectra[30] in the energy range of the exciting laser. For that reason, we used a linear function (Figure 3, dashed lines) to evalute the overlap integral (eq 3). The results are shown in Figures 6 and 7.

■ ANALYTIC DERIVATION OF SECOND-ORDER POWER SPECTRAL DENSITY (PSD)

In this section we provide simple analytic expressions for the second-order power spectral density (PSD) generated by combined GDD and TOD spectral modulation and in addition spectral step modulation of a Gaussian laser pulse. Numerical simulation of the second-order PSD induced by GDD and TOD separately, have already been reported in ref 32.

GDD−TOD Spectral Modulation. As will be presented in the section on the simulated second-order spectra, this type of spectral modulation yields spectrally narrow and tunable second-order spectra (cf., Figure 7), which are especially useful for spectroscopic applications. To be able to employ combined GDD and TOD spectral modulation as a spectroscopic tool, we analyze its properties quantitatively as a function of both modulation parameters ϕ_2 and ϕ_3. Although the *temporal* pulse shape resulting from GDD and TOD spectral modulation has been reported recently to be essentially described by an Airy function[33] of a complex valued argument, for the subsequent derivation we resort to a *spectral* analysis. We start by considering a Gaussian shaped temporal pulse envelope with an intensity fwhm (full width at half maximum) of Δt and a field amplitude of $\mathcal{E}_t$

$$\mathcal{E}(t) = \mathcal{E}_t \cdot e^{-\ln(4)\left(\frac{t}{\Delta t}\right)^2} \tag{9}$$

Accordingly, the spectrum of the unmodulated field envelope reads

$$\tilde{\mathcal{E}}(\omega) = \mathcal{E}_\omega \cdot e^{-\ln(4)\left(\frac{\omega}{\Delta\omega}\right)^2} \tag{10}$$

where the spectral bandwidth (intensity fwhm) of the pulse is

$$\Delta\omega = \frac{4\ln(2)}{\Delta t} \tag{11}$$

with a spectral electric field amplitude of

$$\mathcal{E}_\omega = \mathcal{E}_t \frac{\sqrt{8\pi\ln(2)}}{\Delta\omega} \tag{12}$$

According to eq 2 the modulated second-order spectrum is obtained by spectral convolution of the modulated spectra

$$\tilde{\mathcal{S}}_{\text{mod}}(\omega) = \int_{-\infty}^{+\infty} \tilde{\mathcal{E}}\left(\frac{\omega}{2} + \Omega\right)\tilde{\mathcal{E}}\left(\frac{\omega}{2} - \Omega\right) e^{-i[\varphi(\frac{\omega}{2}+\Omega)+\varphi(\frac{\omega}{2}-\Omega)]}\, d\Omega \tag{13}$$

where we omit all prefactors for simplicity. Inserting the unmodulated Gaussian spectrum (eq 10) and the GDD−TOD spectral modulation function (here taken with reference to the pulse envelope unlike eq 6 in which the laser central frequency is the reference)

$$\varphi(\omega) = \frac{\phi_2}{2}\cdot\omega^2 + \frac{\phi_3}{6}\cdot\omega^3 \tag{14}$$

into eq 13 and recalling that the modulated second-order PSD follows from the spectrum by $\tilde{I}_{\text{mod}}(\omega) = |\tilde{\mathcal{S}}_{\text{mod}}(\omega)|^2$, we obtain the expression for the modulated PSD of the second-order field

dx.doi.org/10.1021/jp4010136 | J. Phys. Chem. C 2013, 117, 11780−11790

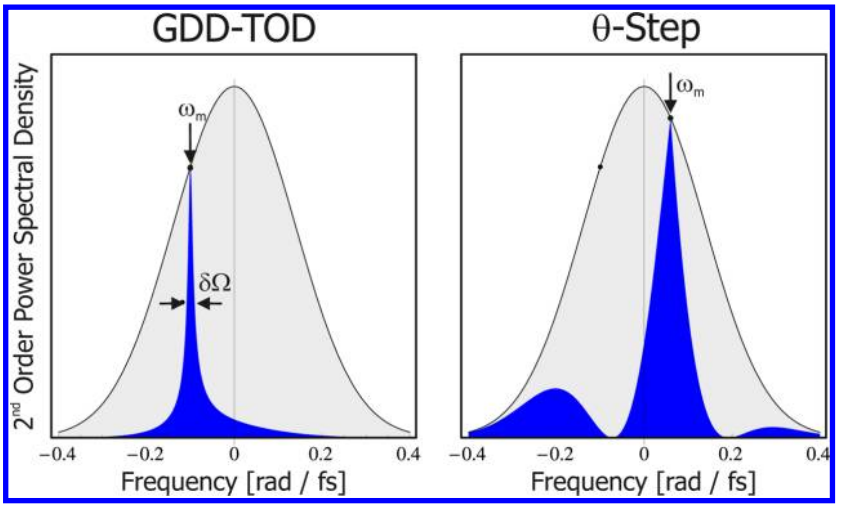

Figure 4. Second-order power spectral density (PSD) for a spectrally phase modulated 12 fs laser pulse. The modulated PSD $\tilde{I}_{mod}(\omega)$ (blue) is always confined within the unmodulated one $\tilde{I}(\omega)$ (gray). Left: Combined GDD and TOD modulation (ϕ_2 = 1000 fs^2 and ϕ_3 = 20000 fs^3). Since the peak intensity at $\omega_m = -2\phi_2/\phi_3$ is controlled by the phase-modulation parameters ϕ_2 and ϕ_3, GDD-TOD modulation is an efficient tool to scan the second-order spectrum with a preselected bandwidth (intensity fwhm) of $\delta\Omega$ by varying ϕ_2 at a given value of ϕ_3. Right: Modulation with a step-function ($\theta = \pi$ and ω_{step} = 0.03 rad/fs). Although the second-order spectrum is also tunable by the step frequency with a maximum at $\omega_m = 2\omega_{step}$, step modulation is much less suitable for spectroscopic applications because of its pronounced side lobes.

$$\tilde{I}_{mod}(\omega) = \frac{\tilde{I}(\omega)}{\sqrt{1 + \left(\frac{\omega - \omega_m}{\Delta\Omega}\right)^2}} \tag{15}$$

where

$$\tilde{I}(\omega) = \frac{\pi \Delta\omega \mathcal{E}_\omega^4}{4\ln(2)} e^{-\ln(4)\left(\frac{\omega}{\Delta\omega}\right)^2} \tag{16}$$

describes the second-order PSD of the unmodulated field

$$\omega_m = -2\frac{\phi_2}{\phi_3} \tag{17}$$

the (approximate, see below) position of the peak in the PSD of the modulated field and $\Delta\Omega = (8\ln(2))/(\phi_3\Delta\omega^2)$ is a measure of its (approximate) spectral width. Because the denominator in eq 15 is always greater (or equal to) one, the modulated PSD $\tilde{I}_{mod}(\omega)$ is always confined within the unmodulated PSD $\tilde{I}(\omega)$ (cf., Figure 4, left). At the frequency $\omega = \omega_m$, the denominator in eq 15 takes its minimum value of one thus maximizing $\tilde{I}_{mod}(\omega)$ provided the unmodulated PSD $\tilde{I}(\omega)$ does not vary significantly within the narrow spectral band $\Delta\Omega$, that is, $\Delta\Omega \ll \Delta\omega$ implying the mnemotechnically more convenient expression $\phi_3 \gg \Delta t^3$ for the above condition. Taking into account the exact form of the spectral profile the intensity fwhm of the modulated spectrum is

$$\delta\Omega = \sqrt{3}\,\Delta\Omega = \frac{8\sqrt{3}\,\ln(2)}{\phi_3\Delta\omega^2} \tag{18}$$

as indicated in the left panel of Figure 4. Since the position of the spectral peak ω_m is controlled by the ratio of ϕ_2 and ϕ_3 (cf., eq 17) and its bandwidth $\delta\Omega$ is determined by ϕ_3 but independent of ϕ_2 (cf., eq 18), combined GDD and TOD phase modulation of the fundamental spectrum provides a convenient tool to scan the second-order spectrum with a preselected bandwidth of $\delta\Omega$ by varying ϕ_2 at a given value of ϕ_3.

Step Modulation. Analytic expressions for the temporal pulse shape because of spectral modulation with a step modulation function have been reported earlier.[34] Here, we present an analytic expression for the second order spectra resulting form spectral modulation by the step modulation function (ω_{step} is taken with reference to the pulse envelope)

$$\varphi(\omega) = \frac{\theta}{2}\sigma(\omega - \omega_{step}) \tag{19}$$

In a manner analogous to the above derivation, we insert the unmodulated Gaussian spectrum (eq 10) and the spectral step modulation function (eq 19) into the spectral convolution (eq 13) to obtain the second-order spectrum

$$\tilde{S}_{mod}(\omega) = \tilde{S}(\omega)\left[1 + (e^{-i\theta} - 1)\mathrm{erf}\left(\sqrt{\ln 2}\,\frac{|\omega - 2\omega_{step}|}{\Delta\omega}\right)\right] \tag{20}$$

where $\tilde{S}(\omega)$ is the unmodulated second-order spectrum and erf describes the error function. The second-order PSD of the modulated field is obtained by

$$\begin{aligned}\tilde{I}_{mod}(\omega) &= |\tilde{S}_{mod}(\omega)|^2 \\ &= \tilde{I}(\omega)\left[1 - 4\sin^2\left(\frac{\theta}{2}\right)\mathrm{erf}(w)\mathrm{erfc}(w)\right]\end{aligned} \tag{21}$$

where w is the dimensionless frequency ratio

$$w = \sqrt{\ln 2}\,\frac{|\omega - 2\omega_{step}|}{\Delta\omega} \tag{22}$$

$\tilde{I}(\omega)$ is the unmodulated second order PSD and $\mathrm{erfc}(w) = 1 - \mathrm{erf}(w)$ the complementary error function. Since $\mathrm{erf}(w)\,\mathrm{erfc}(w) \in [0,1/4]$ for all positive values of w, we see again that the PSD of the modulated field $\tilde{I}_{mod}(\omega)$ is confined within the unmodulated PSD of $\tilde{I}(\omega)$. If the step frequency is well within the spectral bandwidth, that is, $|\omega_{step}| \ll \Delta\omega$ the modulated second-order PSD is characterized by a peak at the position $\omega_m = 2\omega_{step}$ and two side lobes with lower intensity as shown in the right panel of Figure 4. Although the second-order spectrum is

dx.doi.org/10.1021/jp4010136 | J. Phys. Chem. C 2013, 117, 11780−11790

tunable by the step frequency ω_{step}, the intensity of the side lobes increases significantly when the step frequency reaches the wings of the laser spectrum. Therefore, this type of spectral modulation is much less suitable for spectroscopic investigations.

EXPERIMENTAL SECTION

Synthesis of Semiconductor Nanocrystals and Sample Preparation. The colloidal CdS- and CdSe-NCs were synthesized, in the case of the oleic acid (OA)-capped CdS-NCs a well-established method based on a CdO precursor and a weak-coordinating solvent (1-octadecen, ODE) was chosen.[40,41] For the synthesis of the CdSe-NCs, an alternative approach was used, which provided a higher degree of flexibility in the crystal diameter.[42] This approach enabled reproducible size-selective synthesis of CdSe NCs. The CdSe-NCs were capped with bis(2,4,4-trimethylpentyl)phosphonic acid (TMPPA) and trioctylphosphine (TOP). All samples were purified by precipitation with ethanol and redissolved in *n*-hexane for the experiments. The characterization of NCs was carried out by means of UV/vis-absorption and PL spectroscopy. The spectra were obtained by a *Perkin-Elmer* Lambda 40 UV/vis-spectrometer and a *Perkin-Elmer* LS500 luminescence spectrometer from appropriately diluted NC solutions. The absorption spectra (Figure 1a) exhibit well resolved peaks corresponding to optical interband transitions, that originate from the coupling of different electron and hole quantized states. The PL spectrum of the CdSe NCs consists of a narrow single-band centered at 575 nm. The PL spectrum of the CdS NCs shows an intense band, centered at 441 nm but with a white light emission from approximately 480 to 680 nm. This emission is attributed to defect luminescence from surface states. The empirical dependence of the wavelength of the first exciton absorption peak and the nanocrystal diameter d[43,44] allows to calculate the diameter of CdSe-NCs to $d_{CdSe} = 2.9 \pm 0.1$ nm and of CdS-NCs to $d_{CdS} = 4.2 \pm 0.1$ nm. Additionally, the particle concentration c was determined from the absorption of the first excitonic transition and the size-dependent extinction coefficient $\varepsilon(\lambda)$ to $c_{CdSe} = 28 \pm 4$ mM and $c_{CdS} = 13 \pm 2$ mM.[43−45] To study the interaction of both types of NCs with phase shaped laser pulse under exactly the same experimental conditions, a sample containing a mixture of CdSe and CdS NCs was prepared. Solutions of individual NCs were mixed resulting in particle concentrations of $c_{CdSe} = 0.6 \pm 0.1$ mM and $c_{CdS} = 13 \pm 2$ mM. This ratio was chosen to compensate for the lower quantum yield of CdS NCs and may also compensate for an offset in two-photon excitation cross section of the NC types with respect to each other. For the transform-limited pulse, the fluorescence signals of both NCs are approximately of equal magnitude, the corresponding contrast (defined in eq 4) is zero. In addition, care has been taken to ensure low particle concentrations to avoid possible interaction among the NCs and to minimize effects due to radiation reabsorption. The PL of CdSe NCs was detectable nearly background-free against the band-edge emission of CdS NCs (Figure 1).

Setup. The experimental setup is shown schematically in Figure 5. The laser source, a Ti:Saphire oscillator (12 fs, 815 nm, *Femtolasers Femtosource Scientific PRO*) provides pulse energies of 3.5 ± 0.07 nJ at a repetition rate of 75 MHz. The laser power was checked during the complete measurement period by monitoring a 1% fraction of the total beam power, separated with a beam splitter (BS), by a photodiode (PD).

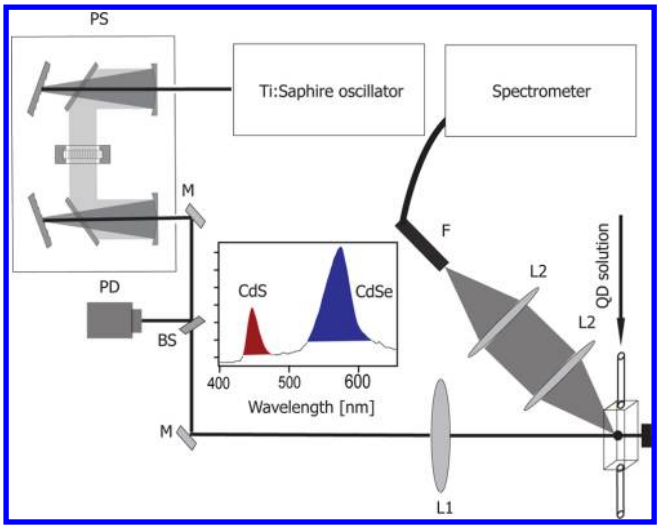

Figure 5. Setup for two-photon excitation of colloidal CdSe and CdS NCs with phase modulated femtosecond laser pulses. PL originating from exciton recombination in both types of NCs is detected simultaneously by a spectrometer. The colored region (inset) corresponds to the spectral integration areas of CdSe (blue) and CdS (red) NCs. The femtosecond laser beam is sent through the liquid-crystal phase modulator (PS) and the laser power is continuously monitored by a photodiode (PD). The diode is irradiated by a fraction of the beam, separated by the beamsplitter (BS). Broadband dielectric mirrors (M) are used to reflect the beam within the optical path. A lens (L1) focuses the beam into a flowcell that contains a circulating solution of both CdSe and CdS NCs. Fluorescence is collected at right angle to the exciting beam via two lenses (L2) and focused onto a fiber bundle (F) linked to an intensified CCD detector located in the exit plane of the spectrometer.

The spectral phase of the laser pulses was modulated using a home-built pulse shaper (PS) based on a liquid crystal spatial light modulator (LC-SLM), described in detail elsewhere.[46] In brief, the shaper is a 4f-zero dispersion compressor consisting of two cylindrical focusing mirrors with a focal length of 75.7 mm and two 830.8 lines per mm reflection gratings (*Thermo RGL Richardson Grating Laboratory*). Each of the 128 pixel of the SLM (*Cambridge Research & Instrumentation, Inc. SLM-128-NIR-PHS*) located in the Fourier plane covers a spectral region of approximately 1.1 nm.

The laser radiation with an average power of 260 mW was focused into a fluorescence flow-cell (quartz, 1 × 1 cm) by a lens (f = 200 mm) to a calculated beam waist of 10.2 mm, resulting in peak intensities of the bandwidth limited (30 fs) pulse (for details see the following section) in the focal region of 66 GW cm^{-2} (maximum in time and space for Gaussian profiles). The PL light from the focal area was collimated using two lenses (f = 100 mm) and focused on the entrance of an optical fiber (diameter 200 μm) coupled to a spectrograph (*Oriel* MS260i, 600 lines/mm grating, *Andor* cooled CCD-camera). To minimize the influence of beam distortions and dispersion along the optical path on the measurement, the focus was positioned directly behind the entrance window.

Measurement. A feedback controlled phase optimization was performed prior to the experiment to compensate for spectral phases introduced by the femtosecond oscillator and the optical components of the setup. To this end the phase sensitivity of the nonlinear fluorescence signal generated by a broadband absorbing dye solution (rhodamine 6G in ethanol) was used as a feedback signal for an evolutionary alogrithm.

dx.doi.org/10.1021/jp4010136 | J. Phys. Chem. C 2013, 117, 11780−11790

The spectral phase at the maximum signal (indicating an optimal, i.e., flat, spectral phase) was introduced for compensation in the subsequent measurements. The pulse compression procedure was validated by direct time domain pulse characterization employing second order interferometric autocorrelation (AC). For this purpose, a double pulse sequence synthesized by a spectral phase comb on the pulse shaper was generated.[47] From the AC trace, one determines the pulse duration and the residual phase in the interaction region to be (29 ± 2) fs and a chirp of 50 fs^2 by a nonlinear fitting procedure. The longer pulse duration results from a loss of bandwidth in the pulse shaper, rather than from the residual phase. Additionally a GDD−TOD [corresponds to the spectral phase function (eq 6) by varying (ϕ_2,ϕ_3) landscape,[33] which is very sensitive to residual phases, was recorded with the dye solution as sample. Beside checking for residual phases, this landscape allowed us to determine the central-frequency ω_0 of the laser spectrum to be 2.311 rad/fs (815 nm). In the experiment, the dye solution was replaced by the NC solution without further readjustment of the optical setup. Before and after the measurements absorption spectra were recorded, displaying no indications of sample degradation during the experiment. A scan of the incident laser radiation in the range of 0.8−2 nJ (at the sample) revealed a nearly quadratic power law (exponent = 1.9) of the NC PL, indicating the two-photon nature of the absorption-process.

In the CC experiment, step modulation and GDD-TOD landscapes were recorded for the NC sample, that is, the two-photon induced PL spectra were recorded for various combinations of the parameters (ω_{step},θ) and (ϕ_2,ϕ_3). From the measured spectra, the integrated PL signals $S^{(2)}$ were derived by integration of the signal in the spectral bands (430−470) nm corresponding to CdS NCs and (530−610) nm corresponding to CdSe NCs, respectively. These signals will be presented in the following section in terms of two-dimensional landscapes.

RESULTS AND DISCUSSION

To analyze the dependence of the PL signal on the phase of the shaped laser pulses and to compare with the experimental results, numerical simulations are performed. In the first part of this section, we consider numerical simulations of the second-order optical spectra for both spectral phase functions (eqs 5 and 6). Analytic expressions for the second-order optical spectra resulting from both types of spectral phase modulation are presented in a separate section. The spectral overlap described by eq 3 is evaluated and control landscapes for different two-photon excitation spectra, based on literature values for CdSe and CdS NCs are calculated.[48,49] In the second part, experimentally obtained landscapes are compared to the simulations discussed in the first part.

Simulation. Figure 6a−d displays simulated signals of $S^{(2)}(\omega_{step},\theta)$ according to eq 3. The results were obtained with four different slopes used to approximate the two-photon excitation spectra. Note that a slope of 0 eV^{-1} (a) corresponds to the two-photon excitation spectrum of the CdSe NCs as reported by ref 31, whereas the slope with 1.3 eV^{-1} (c) corresponds to that of the CdS NCs.[30] Increasing the slope of the two-photon excitation spectra causes a more pronounced minimum in the landscape around (ω_{step},θ) = 2.4 rad/fs, 4 rad). In this region, the simulated control landscapes of CdSe and CdS NCs are different for this type of phase modulation. The transform limited (TL) pulse generates the maximum signal

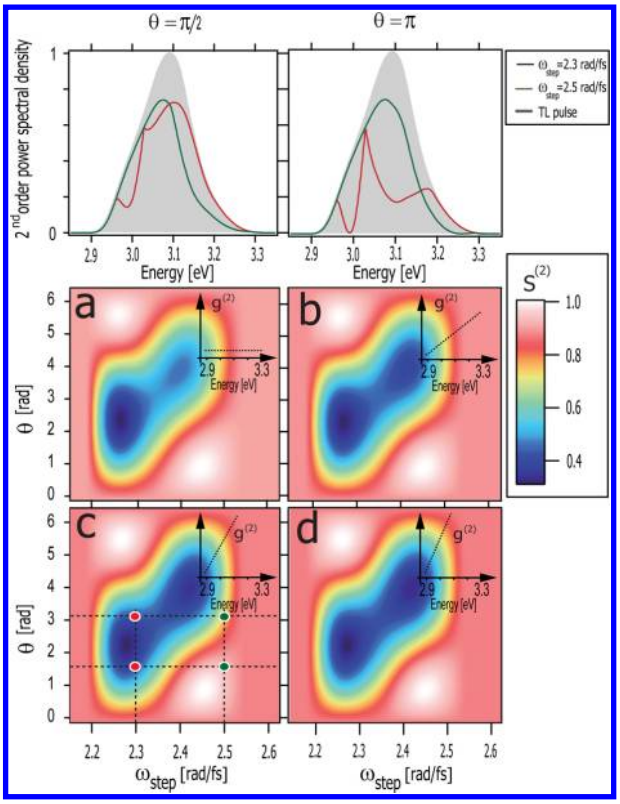

Figure 6. Upper graphs: Simulated second order spectra (in units of 2 ω_{step}) of the transform limited input pulse (shaded), as well as for selected step modulation parameters. Dotted straight lines (upper graph right) represent linear approximated two-photon excitation spectra $g^{(2)}(\omega)$ with slopes of (a) 0, (b) 0.6, (c) 1.3, and (d) 1.6 eV^{-1}. The landscapes below display the corresponding simulations of the integrated signal $S^{(2)}(\omega_{step},\theta)$ as a function of the step frequency ω_{step} and the modulation depth θ, for the individual slopes. Points of distinct parameter combinations leading to the second-order spectra displayed above are highlighted by dots in landscape (c).

that usually is obtained at step-frequencies located outside the spectrum. Inclusion of the experimentally verified residual spectral phase leads to the appearance of the two maxima in each landscape. Therefore, this phase has also been considered in the simulations shown above. The amplitude-modulated second-order spectra $\tilde{S}_{mod}(\omega - 2\omega_0)$ for the step modulation function at $\theta = \pi/2$ and $\theta = \pi$ are displayed for two selected step frequencies, indicated by points in landscape (c). If the step is located in the wings of the laser spectrum (ω_{step} = 2.5 rad/fs), the resulting second-order spectrum is only weakly modulated. Generally the spectra exhibit a triple humped shape (see Figure 4), which limits the spectral resolution. If ω_{step} is equal to the central frequency, the strongest modulation of the second-order optical spectrum is obtained. However, because of the triple hump structure this feature is not highly spectrally selective and cannot be tuned efficiently across the full bandwidth of the TL pulse (Figure 6 upper graph). On the basis of the simulation, the achievable contrast in the excitation of CdSe and CdS NCs is around 0.15 (see below, for instance in Figure 8).

In the following, we consider the other spectral phase modulation function (GDD−TOD) to provide high spectral selectivity. Combined GDD and TOD spectral phase modulation yields a narrow second-order spectrum (peak) with a well-defined maximum at $\omega_m = 2(\omega_0 - \phi_2/\phi_3)$, that is

dx.doi.org/10.1021/jp4010136 | J. Phys. Chem. C 2013, 117, 11780−11790

adjustable by the choice of (ϕ_2,ϕ_3). In particular, increasing the GDD allows "scanning" of the amplitude modulated second order spectrum (Figure 7 upper graphs). If the sign of the TOD

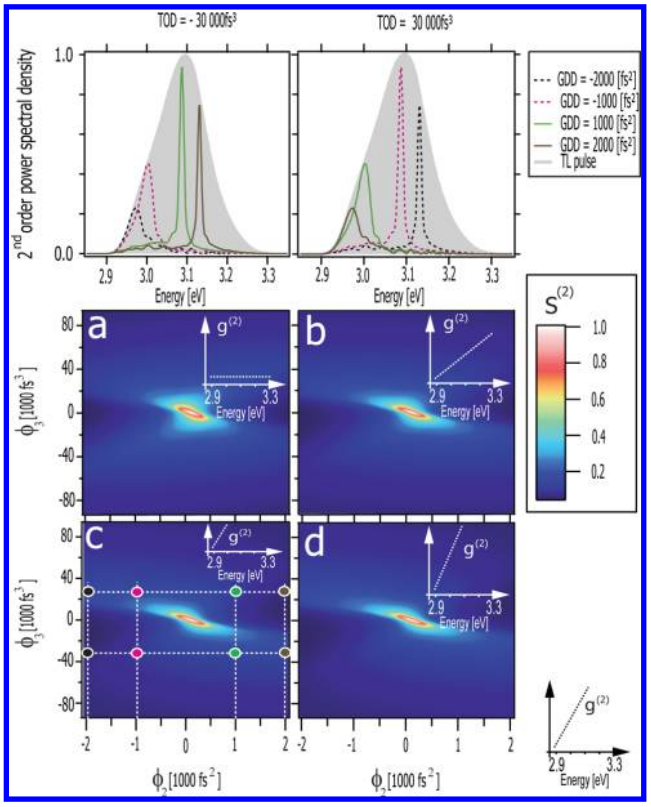

Figure 7. Same as in Figure 6 for various GDD and TOD phase modulation parameters. In contrast to the step-modulation various combinations of parameters lead to narrow and spectrally tunable second-order spectra, capable of efficiently scanning the two-photon excitation spectra $g^{(2)}$ associated with the slopes a–d. The slope of $g^{(2)}$ used for computation of landscape c is indicated because of limited space as symbol in the landscape and magnified on the right-hand side at the bottom of the figure.

phase is inverted, the position of the second order spectral peak is shifted from the "red" to the "blue" part of the spectrum or vice versa. The background in the spectra is much weaker compared to the step modulation. In Figure 7a–d, a similar representation was chosen for the PL signals $S^{(2)}(\phi_2,\phi_3)$ from combined GDD and TOD phase modulation.

Assuming a flat two-photon excitation spectrum of the NCs a slightly tilted "butterfly" shape was obtained for the landscape (a). For an ideally Gaussian spectrum, the laser central frequency is well-defined, thus a perfectly symmetric shape of the landscape would be obtained. As our experimental spectrum also used in the simulations above is not symmetric, the accuracy in determing ω_0 is limited, leading to an initial minor tilt. The high spectral resolution manifests in the contrast of the control landscapes, which is calculated to 0.4 being significantly higher than for the step modulation. For larger slopes, the landscapes become asymmetric, that is, the intensity in one of the diagonal directions decreases. The overlap of the spectral peak with the two-photon excitation spectrum $g^{(2)}(\omega)$ (slope >0) is larger in the blue part of the second-order spectrum compared to the respective red part. Therefore the signal is higher in the blue part of the second-order spectrum.

Comparison of Experiment and Simulation. In this section, we compare the experimentally obtained landscape with the simulations described above starting with the step modulation and then considering the results of GDD–TOD modulation. A typical measured control landscape of two-photon induced NC luminescence, consists of an array of (41 × 41) single measurements (Figure 8a, b). The frequency ω_{step} of

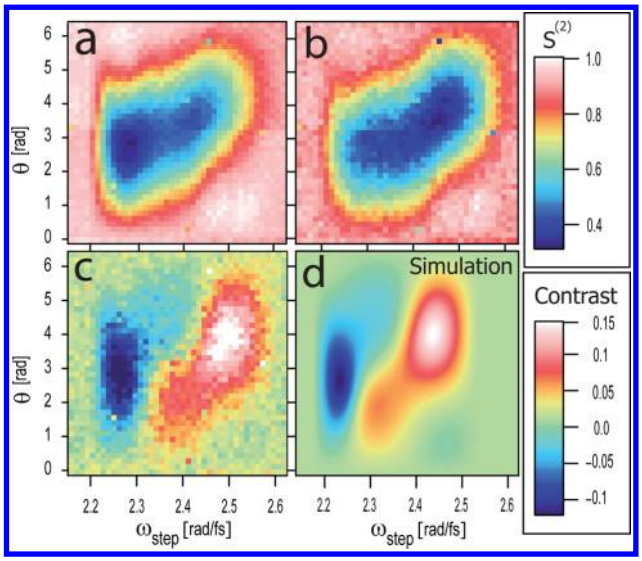

Figure 8. Control by step modulation. Control landscapes of two-photon induced recombination Pl of the band-edge exciton from 2.9 nm CdSe NCs (detected in the spectral range 530–610 nm) (a) and from 4.2 nm CdS NCs (detected in the spectral range 430–470 nm) (b). The integrated signals $S^{(2)}(\omega_{step},\theta)_{CdSe}$ and $S^{(2)}(\omega_{step},\theta)_{CdS}$ arising for the step modulation are normalized to the landscape maximum. The contrast of $S^{(2)}(\omega_{step},\theta)_{CdSe}$ and $S^{(2)}(\omega_{step},\theta)_{CdS}$ according to eq 4 (c), is shown along with the corresponding simulation (d).

the step modulation is varied on the horizontal axis from 2.2 to 2.6 rad/fs corresponding to a wavelength range from 856 to 725 nm and the modulation depth θ from 0 to 2π on the vertical axis. The signal intensity decreased for frequencies in the vicinity of the central frequency for both CdSe and CdS NCs. However the signal decrease for CdSe NCs is more pronounced in the red part (low-step frequencies) of the laser spectrum compared to CdS NCs. Their signal features a stronger decrease in the blue part (high step frequencies). This observation agrees with the results of our simulations (Figure 6a, c). The simulated control landscape (Figure 6a) was obtained for the slope of 0 eV^{-1} of the two-photon excitation spectrum (CdSe), whereas (Figure 6c) was obtained for the slope of 1.3 eV^{-1} (CdS). The two areas with the highest signal in the lower right and upper left corners of the landscapes (Figure 6a–d) result from an additional quadratic phase of 50 fs^2, which was included in the simulations. For better comparison, we show the measured landscapes of CdSe NCs (Figure 8a) and CdS NCs (Figure 8b) along with the contrast of the measurements (Figure 8c) and the simulated contrast (Figure 8d). The maximum contrast obtainable for the step modulation is 0.15.

Figure 9a and b shows control landscapes of luminescence for GDD–TOD modulated laser pulses for both NC types. The GDD was varied from −2000 to 2000 fs^2 on the horizontal axis (41 points). Values of TOD ranging from -90×10^3 to 90×10^3 fs^3 were displayed on the vertical axis (41 points).

dx.doi.org/10.1021/jp4010136 | J. Phys. Chem. C 2013, 117, 11780–11790

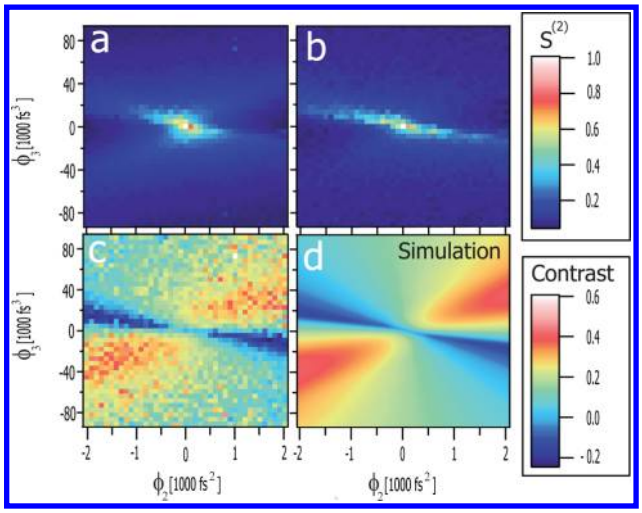

Figure 9. Control by GDD−TOD phase modulation. The same as in Figure 8 but for GDD-TOD modulated pulses. The two-photon induced luminescence from CdSe NCs leads to an almost symmetric landscape (a), whereas in the case of CdS NCs the asymmetry of the landscape is more pronounced (b). The contrast of panels a and b is presented in panel c. The simulated contrast (d) is calculated from the landscapes in Figure 7a−c.

Spectral phase modulation by GDD and TOD led to a nearly symmetric shape of the CdSe NCs control landscape (Figure 9a). In contrast, the landscape of CdS NCs (Figure 9b) features a significant distortion along the diagonal directions. The experimental contrast (defined analogously to eq 4) is presented in (Figure 9c), along with the simulation of the contrast in (Figure 9d).

The obtained contrast using GDD−TOD modulated pulses was quantified to be 0.4. This observation can be explained by the shape of the computed second-order optical spectra, that result from GDD−TOD modulation. The spectral energy is efficiently concentrated to frequencies being different suitable for the excitation of either CdSe or CdS NCs. The magnitude of the contrast in the simulated landscapes, as well as their structures are in agreement with the experimental data. For both types of modulation it was observed that areas of contrast suppression and enhancement are present in the experimental, as well as in the simulated data. In both cases, the landscapes are found to be insensitive to the spectral integration range within the inhomogeneous broadened PL band of an individual material system. This means that integration over the wavelength ranges 530−540 nm (blue part of CdSe NCs emission) or 600−610 nm (red part of CdSe emission) leads to the same landscape. The same observation was made for the CdS NCs in the wavelength ranges 430−440 and 460−470 nm. The agreement of experimental and simulated results for both NCs indicates that the two-photon excitation spectra of the NCs are responsible for the difference in the observed spectral phase-dependence of both modulation functions. In addition to the experimental data presented, the measurements were repeated utilizing complementary control systems, such as CdSe NCs of mean diameters 2.3, 3.9, 4.5, and 6.9 nm and a broadband absorbing dye for reference. The observed control landscapes do not vary significantly upon variation of the NC diameter and are identical to the landscapes obtained from the dye. For further comparison, control landscapes were measured also on commercial CdSe and CdS NCs (Lumidot CdSe510,CdS420) purchased from Sigma Aldrich, the resulting control landscapes show the same differences for CdSe and CdS NCs as those presented in Figures 8 and 9a−c. While modification of the NC size alters the linear spectra, the two-photon spectra of the NC-ensembles are apparently not influenced in the spectral range, accessible with our femtosecond laser. Therefore variation of the crystal diameter is not sufficient for obtaining a phase sensitive nanoprobe for selective two-photon excitation with shaped fs laser pulses. Moreover, repeating the experiments with a solid NC sample (NCs dispersed in PMMA) under cryogenic conditions (35 K) also revealed no significant differences in the landscapes obtained at room-temperature.

■ CONCLUSIONS

We have shown that ensembles of CdSe and CdS NCs in a single sample can be selectively excited by shaped femtosecond laser pulses in the liquid phase. The observed selectivity relies on different two-photon excitation spectra and on higher-order spectral interference of the shaped pulses. The experimental results were reproduced with the corresponding model. Processes like multiexciton or excited state absorption are not required to rationalize our experimental findings. Selectivity of excitation was not observed within the same material system. Nanocrystals can thus be used for coherently controlled two-photon microscopy under ambient conditions taking advantage of their high photostability. The properties of two spectral phase modulation functions, that is, the θ-step and GDD-TOD were investigated as a spectroscopic tool to scan the two-photon excitation spectra of nanocrystals. It turns out that modulation by combined GDD and TOD provides a more sensitive tool for scanning than the established θ-step.

■ AUTHOR INFORMATION

Corresponding Author

*E-mail: baumert@physik.uni-kassel.de.

Notes

The authors declare no competing financial interest.

■ ACKNOWLEDGMENTS

We gratefully acknowledge the Deutsche Forschungsgemeinschaft DFG (German Research Foundation) for founding the research. We would like to thank Dr. T. Bayer for the fruitful discussions and Prof. J. P. Reithmaier (University Kassel) for providing additional low temperature equipment.

■ REFERENCES

(1) Zewail, A. H. *Femtochemistry*; World Scientific Publishing Co., Pte., Ltd.: Singapore, 1994.

(2) Shapiro, M., Brumer, P. *Quantum Control of Molecular Processes*, 2nd ed.; Wiley-VCH: Berlin, Germany, 2011.

(3) Wollenhaupt, M.; Baumert, T. Ultrafast Laser Control of Electron Dynamics in Atoms, Molecules and Solids. *Faraday Discuss.* **2011**, *153*, 9−26, DOI: 10.1039/c1fd00109d.

(4) Chuntonov, L.; Rybak, L.; Gandman, A.; Amitay, Z. Frequency-Domain Coherent Control of Femtosecond Two-Photon Absorption: Intermediate-Field vs. Weak-Field Regime. *J. Phys. B: At. Mol. Opt. Phys.* **2008**, No. 035504, DOI: 10.1088/0953-4075/41/3/035504.

(5) Broers, B.; Noordam, L. D.; van Linden, H. B.; van den Heuvell, H. Diffraction and Focusing of Spectral Energy in Multiphoton Processes. B. *Phys. Rev. A* **1992**, *46*, 2749−2756, DOI: 10.1103/PhysRevA.46.2749.

(6) Blanchet, V.; Nicole, C.; Bouchene, M.-A.; Girard, B. Temporal Coherent Control in Two-Photon Transitions: From Optical

Interferences to Quantum Interferences. *Phys. Rev. Lett.* **1997**, *78*, 2716−2719, DOI: 10.1103/PhysRevLett.78.2716.
(7) Meshulach, D.; Silberberg, Y. Coherent Quantum Control of Two-Photon Transitions by a Femtosecond Laser Pulse. *Nature* **1998**, *396*, 239−242, DOI: 10.1038/24329.
(8) Präkelt, A.; Wollenhaupt, M.; Sarpe-Tudoran, C.; Baumert, T. Phase Control of a Two-Photon Transition with Shaped Femtosecond Laser-Pulse Sequences. *Phys. Rev. A* **2004**, *70*, 063407-1−063407-10, DOI: 10.1103/PhysRevA.70.063407.
(9) Cerullo, V.; Bardeen, C. J.; Wang, Q.; Shank, C. V. High-Power Femtosecond Chirped Pulse Excitation of Molecules in Solution. *Chem. Phys. Lett.* **1996**, *262*, 362−368, DOI: 10.1016/0009-2614(96)01092-5.
(10) Ogilvie, J. P.; Debarre, D.; Solinas, X.; Martin, J. L.; Beaurepaire, E.; Joffre, M. Use of Coherent Control for Selective Two-Photon Fluorescence Microscopy in Live Organisms. *Opt. Express* **2006**, *14*, 759−766.
(11) Nuernberger, P.; Vogt, G.; Brixner, T.; Gerber, G. Femtosecond Quantum Control of Molecular Dynamics in the Condensed Phase. *Phys. Chem. Chem. Phys.* **2007**, *9*, 2470−2497, DOI: 10.1039/B618760A.
(12) Roth, M.; Guyon, L.; Roslund, J.; Boutou, V.; Courvoisier, F.; Wolf, J.-P.; Rabitz, H. Quantum Control of Tightly Competitive Product Channels. *Phys. Rev. Lett.* **2009**, *102*, 253001-1−253001-4, DOI: 10.1103/PhysRevLett.102.253001.
(13) Xu, B.; Coello, Y.; Lozovoy, V. V.; Dantus, M. Two-Photon Fluorescence Excitation Spectroscopy by Pulse Shaping Ultrabroad-Bandwidth Femtosecond Laser Pulses. *Appl. Opt.* **2010**, *49*, 6348−6353.
(14) Gerber, G.; Brixner, T. Quantum Control of Gas-Phase and Liquid-Phase Femtochemistry. *Chem. Phys. Chem.* **2003**, *4*, 418−438, DOI: 10.1002/cphc.200200581.
(15) Brixner, T.; Stenger, J.; Vaswani, H. M.; Cho, M.; Blankenship, R. E.; Fleming, G. R. Femtochemistry and Femtobiology, Ultrafast Events in Molecular Science. *Nature* **2005**, *434*, 625−628.
(16) Buckup, T.; Hauer, J.; Moehring, J.; Motzkus, M. Multidimensional Spectroscopy of Beta-Carotene: Vibrational Cooling in the Excited State. *Arch. Biochem. Biophys.* **2009**, *483*, 219−223, DOI: 10.1016/j.abb.2008.10.031.
(17) Moran, S. D.; Decatur, S. M.; Zanni, M. T. Structural and Sequence Analysis of the Human γD-Crystallin Amyloid Fibril Core Using 2D IR Spectroscopy, Segmental ^{13}C Labeling, and Mass Spectrometry. *J. Am. Chem. Soc.* **2012**, *134*, 18410−18416, DOI: 10.1021/ja307898g.
(18) Gdor, I.; Sachs, H.; Roitblat, A.; Strasfeld, D. B.; Bawendi, M. G.; Ruhman, S. Exploring Exciton Relaxation and Multiexciton Generation in PbSe Nanocrystals Using Hyperspectral Near-IR Probing. *ACS Nano* **2012**, *6*, 3269−3277, DOI: 10.1021/nn300184n.
(19) Simon, C.-M.; Belhadj, T.; Chatel, B.; Amand, T.; Renucci, P.; Lemaitre, A.; Krebs, O.; Dalgarno, P. A.; Warburton, R. J.; Marie, X.; Urbaszek, B. Robust Quantum Dot Exciton Generation via Adiabatic Passage with Frequency-Swept Optical Pulses. *Phys. Rev. Lett.* **2011**, *106*, 166801 DOI: 10.1103/PhysRevLett.106.166801.
(20) Zdobnova, T.; Dorofeev, S.; Tananaev, P.; Vasiliev, R.; Balandin, T.; Edelweiss, E.; Stremovskiy, O.; Balalaeva, I.; Turchin, I.; Lebedenko, E.; Zlomanov, V.; Deyev, S. Fluorescent Immunolabeling of Cancer Cells by Quantum Dots and Antibody scFv Fragment. *J. Biomed. Opt.* **2009**, *14*, 021004 DOI: 10.1117/1.3122775.
(21) Deerinck, T. J. The Application of Fluorescent Quantum Dots to Confocal, Multiphoton, and Electron Microscopic Imaging. *Toxicol. Pathol.* **2008**, *36*, 112−116, DOI: 10.1177/0192623307310950.
(22) Gaponeko, S. V.; Woggon, U. Excitons in Quantum Dots. *Phys. Status Solidi B* **1995**, *189*, 285 DOI: 10.1002/pssb. 2221890202.
(23) Schmidt, M. E.; Blanton, S. A.; Hines, M. A.; Guyot-Sionnest, P. Size-Dependent Two-Photon Excitation Spectroscopy of CdSe Nanocrystals. *Phys. Rev. B* **1996**, *53*, 12629−12632, DOI: 10.1103/PhysRevB.53.12629.
(24) Tomassi, R.; Lepore, M.; Ferrara, M.; Catalano, M. Observation of High-Index States in $CdS_{1-x}Se_x$ Semiconductor Microcrystallites by Two-Photon Spectroscopy. *Phys. Rev. B* **1992**, *46*, 12261−12265, DOI: 10.1103/PhysRevB.46.12261.
(25) Adachi, S. *Properties of Group-IV, III-V and II-VI Semiconductors*, 1st ed.; Wiley-VCH: Weinheim, Germany, 2005.
(26) Delysse, S.; Filloux, P.; Dumacher, V.; Fiorini, C.; Nunzi, J.-M. Multiphoton Absorption in Organic Dye Solutions. *Opt. Mater.* **1998**, *9*, 347−351, DOI: 10.1016/S0925-3467(97)00101-8.
(27) Efros, A. L; Lockwood, D. J.; Tsybeskov, L. *Semiconductor Nanocrystals*; Kluwer Academic: Amsterdam, the Netherlands, 2002.
(28) Kambhampati, P. Unraveling the Structure and Dynamics of Excitons in Semiconductor Quantum Dots. *Acc. Chem. Res.* **2010**, *44*, 1−13, DOI: 10.1021/ar1000428.
(29) Kambhampati, P. Multiexcitons in Semiconductor Nanocrystals: A Platform for Optoelectronics at High Carrier Concentration. *Phys. Chem. Lett.* **2012**, *3*, 1182−1190, DOI: 10.1021/jz300239j.
(30) Li, X.; van Emden, J.; Chon, J. W. M.; Gu, M. Enhanced Two-Photon Absorption of CdS Nanocrystal Rods. *Appl. Phys. Lett.* **2009**, *94*, 103117 DOI: 10.1063/1.3100196.
(31) Feng, X.; Ji, W. Shape-Dependent Two-Photon Absorption in Semiconductor Nanocrystals. *Opt. Express* **2009**, *17* (15), 13140−13150, DOI: 10.1364/OE.17.013140.
(32) Lozovoy, V. V.; Pastirk, I.; Walowicz, K. A.; Dantus, M. Multiphoton Intrapulse Interference. II. Control of Two- and Three-Photon Laser Induced Fluorescence with Shaped Pulses. *J. Chem. Phys.* **2003**, *118* (7), 3187−3196, DOI: 10.1063/1.1531620.
(33) Schneider, J.; Wollenhaupt, M.; Winzenburg, A.; Bayer, T.; Köhler, J.; Faust, R.; Baumert, T. Efficient and Robust Strong-Field Control of Population Transfer in Sensitizer Dyes with Designed Femtosecond Laser Pulses. *Phys. Chem. Chem. Phys.* **2011**, *13*, 8733−8746, DOI: 10.1039/c0cp02723e.
(34) Wollenhaupt, M.; Bayer, T.; Vitanov, V. V.; Baumert, T. Three-State Selective Population of Dressed States via Generalized Spectral Phase-Step Modulation. *Phys. Rev. A* **2010**, *81*, 053422-1−053422-9, DOI: 10.1103/PhysRevA.81.053422.
(35) Weiner, A. M. Femtosecond Pulse Shaping Using Spatial Light Modulators. *Rev. Sci. Instrum.* **2000**, *71*, 1929−1958, DOI: 10.1063/1.1150614.
(36) Wollenhaupt, M. In *Springer Handbook of Lasers*, 1st ed.; Springer: New York, NY, U.S.A., 2007.
(37) Boyd, R. W. *Nonlinear Optics*, 2nd ed.; Elsevier Science: Boston, MA, U.S.A., 2003.
(38) Bayer, T.; Wollenhaupt, M.; Sarpe-Tudoran, C.; Baumert, T. Robust Photon Locking. *Phys. Rev. Lett.* **2009**, *102*, 023004−023200.
(39) Zhang, Z.; Zhang, H.; Yang, Y.; Jia, T.; Wang, Z.; Sun, Z. Coherent Enhancement in Two-Photon Fluorescence in Molecular System Induced by Phase-Jump Modulated Pulse. *J. Chem. Phys.* **2010**, *132*, 094503-1−094503-4, DOI: 10.1063/1.3327843.
(40) Peng, Z. A.; Peng, X. Formation of High-Quality CdTe, CdSe, and CdS Nanocrystals Using CdO as Precursor. *J. Am. Chem. Soc.* **2001**, *123*, 183−184, DOI: 10.1021/ja003633m.
(41) Yu, W. W.; Peng, X. Formation of High-Quality CdS and Other II−VI Semiconductor Nanocrystals in Noncoordinating Solvents: Tunable Reactivity of Monomers. *Angew. Chem., Int. Ed.* **2002**, *41* (13), 2368−2371.
(42) van Embden, J.; Mulvaney, P. Nucleation and Growth of CdSe Nanocrystals in a Binary Ligand System. *Langmuir* **2005**, *21*, 10226−10233, DOI: 10.1021/la0510811.
(43) Yu, W. W.; Qu, L.; Guo, W.; Peng, X. Experimental Determination of the Extinction Coefficient of CdTe, CdSe, and CdS Nanocrystals. *Chem. Mater.* **2003**, *15*, 2854−2860, DOI: 10.1021/cm034081k.
(44) Yu, W. W.; Qu, L.; Guo, W.; Peng, X. Experimental Determination of the Extinction Coefficient of CdTe, CdSe and CdS Nanocrystals. *Chem. Mater.* **2004**, *16*, 560 DOI: 10.1021/cm033007z.
(45) Jasieniak, J.; Smith, L.; van Embden, J.; Mulvaney, P.; Califano, M. Re-examination of the Size-Dependent Absorption Properties of CdSe Quantum Dots. *J. Phys. Chem. C* **2009**, *113*, 19468−19474, DOI: 10.1021/jp906827m.

(46) Präkelt, A.; Wollenhaupt, M.; Assion, A.; Horn, C.; Sarpe-Tudoran, C.; Winter, C.; Baumert, T. Compact, robust, and flexible setup for femtosecond pulse shaping. *Rev. Sci. Instrum.* **2003**, *74* (11), 4950−4953, DOI: 10.1063/1.1611998.
(47) Pestov, D.; Lozovoy, V. V.; Dantus, M. Multiple Independent Comb Shaping (MICS): Phase-Only Generation of Optical Pulse Sequences. *Opt. Express* **2009**, *17* (16), 14351−14361.
(48) Walowicz, K. A.; Pastirk, I.; Lozovoy, V. V.; Dantus, M. Multiphoton Intrapulse Interference. 1. Control of Multiphoton Processes in Condensed Phases. *J. Phys. Chem. A* **2002**, *106*, 9369−9373, DOI: 10.1021/jp0258964.
(49) Oron, D.; Dudovich, N.; Silberberg, Y. Coherence and Control in Chemistry. *Faraday Discuss.* **2011**, *153*, 293−319, DOI: 10.1039/C1FD90027G.